HHS Public Access

Author manuscript

Nat Chem Biol. Author manuscript; available in PMC 2021 July 18.

Published in final edited form as:

Nat Chem Biol. 2021 April ; 17(4): 412–420. doi:10.1038/s41589-020-00715-0.

Structure of Erm-modified 70S ribosome reveals the mechanism of macrolide resistance.

Maxim S. Svetlov[1,2,6], **Egor A. Syroegin**[3,6], **Elena V. Aleksandrova**[3], **Gemma C. Atkinson**[4], **Steven T. Gregory**[5], **Alexander S. Mankin**[1,2], **Yury S. Polikanov**[1,2,3,#]

[1]Center for Biomolecular Sciences, University of Illinois at Chicago, Chicago, IL 60607, USA

[2]Department of Pharmaceutical Sciences, University of Illinois at Chicago, Chicago, IL 60607, USA

[3]Department of Biological Sciences, University of Illinois at Chicago, Chicago, IL 60607, USA

[4]Department of Molecular Biology, Umeå University, 901 87 Umeå, Sweden

[5]Department of Cell and Molecular Biology, University of Rhode Island, Kingston, RI 02881, USA

[6]These authors contributed equally to this work: Maxim S. Svetlov, Egor A. Syroegin

Abstract

Many antibiotics inhibit bacterial growth by binding to the ribosome and interfering with protein biosynthesis. Macrolides represent one of the most successful classes of ribosome-targeting antibiotics. The main clinically-relevant mechanism of resistance to macrolides is dimethylation of the 23S rRNA nucleotide A2058 located in the drug binding site, a reaction catalyzed by the Erm-type rRNA-methyltransferases. Here, we present the crystal structure of the Erm-dimethylated 70S ribosome at 2.4Å resolution together with the structures of unmethylated 70S ribosome functional

[#]Correspondence: yuryp@uic.edu (Y.S.P.).

AUTHOR CONTRIBUTIONS

M.S.S. with the help from S.T.G. constructed the *T. thermophilus* HB27 strain expressing Erm-like methyltransferase; M.S.S. performed the assessment of A2058-methylation; M.S.S and E.A.S. grew *T. thermophilus* cells and purified A2058-methylated and unmethylated 70S ribosomes; E.A.S. and E.V.A. prepared hydrolysis-resistant aminoacylated tRNAs; M.S.S., E.A.S., E.V.A., and Y.S.P designed and performed X-ray crystallography experiments; A.S.M. and Y.S.P. supervised the experiments. G.C.A performed phylogenetic analysis and predicted thermostable *erm* genes. All authors interpreted the results. M.S.S., S.T.G., A.S.M., and Y.S.P. wrote the manuscript.

DATA AVAILABILITY STATEMENT

Coordinates and structure factors were deposited in the RCSB Protein Data Bank with accession codes: **6XHV** for the A2058-dimethylated *T. thermophilus* 70S ribosome in complex with mRNA, aminoacylated A-site Phe-NH-tRNA^{Phe}, aminoacylated P-site fMet-NH-tRNA$_i^{Met}$, and deacylated E-site tRNA^{Phe}; **6XHW** for the A2058-unmethylated *T. thermophilus* 70S ribosome in complex with mRNA, aminoacylated A-site Phe-NH-tRNA^{Phe}, aminoacylated P-site fMet-NH-tRNA$_i^{Met}$, and deacylated E-site tRNA^{Phe}; **6XHX** for the *T. thermophilus* 70S ribosome in complex with erythromycin and protein Y; **6XHY** for the *T. thermophilus* 70S ribosome in complex with telithromycin, mRNA, aminoacylated A-site Phe-NH-tRNA^{Phe}, aminoacylated P-site fMet-NH-tRNA$_i^{Met}$, and deacylated E-site tRNA^{Phe}.

All previously published structures that were used in this work for structural comparisons were retrieved from the RCSB Protein Data Bank: PDB entries 1VY4, 6ND6, 4V7U, 4V7V, 4V7X, 4V7Y, 4V7Z, 1YI2, 1YHQ, 1YIJ, 4U26.

No sequence data were generated in this study. Analyzed protein sequences are presented with their corresponding accession numbers in the phylogenetic tree (Supplementary Fig. 1) for retrieval from the NCBI protein database.

COMPETING FINANCIAL INTERESTS STATEMENT

The authors declare no competing financial interests.

complexes alone and in combination with macrolides. Altogether, our structural data do not support the previous models and, instead, suggest a principally new explanation of how A2058-dimethylation confers resistance to macrolides. Moreover, high-resolution structures of two macrolide antibiotics bound to the unmodified ribosome revealed a previously unknown role of desosamine moiety in drug binding, laying a foundation for the rational knowledge-based design of macrolides that can overcome Erm-mediated resistance.

Keywords

Macrolide; antibiotic; resistance; methylation; A2058; 23S rRNA; 70S ribosome; X-ray structure; inhibition of translation; peptidyl transferase center; nascent peptide exit tunnel

INTRODUCTION

Antibiotics prevent bacterial growth by inhibition of vital cellular processes. Many of them target functionally important sites on the bacterial 70S ribosome and block protein synthesis[1]. Prominent among these inhibitors are macrolide antibiotics, a large family of natural and semi-synthetic compounds that consist of 12- to 16-membered macrolactone rings decorated with various side chains. Macrolides are widely used for the treatment of human community-acquired bacterial respiratory tract infections, including those that arise as complications of viral diseases[2,3]. These antibacterials achieve their inhibitory action by binding in the nascent peptide exit tunnel (NPET) of the bacterial ribosome and interfering with the progression of some growing polypeptides through this tunnel[4]. Several mechanisms of resistance to macrolides have been described, including efflux[5,6], enzymatic degradation of the drugs[7,8], or alteration of the drug-binding pocket through mutations[6,9]. However, the most abundant among bacterial pathogens and clinically most relevant mechanism of resistance against macrolides is based on mono- or dimethylation of the N6 position of a specific adenine residue (A2058) of the 23S rRNA (*E. coli* numbering of the nucleotides is used throughout) (Fig. 1a)[10–12]. The modification of this nucleotide located in the macrolide binding pocket in the NPET is catalyzed by the Erm-type rRNA methyltransferases[13,14]. Dimethylation, in particular, dramatically reduces the binding of the macrolides to the ribosome, rendering cells highly resistant to these drugs[15,16]. In addition to macrolides, the same modification confers resistance to two other structurally-unrelated classes of ribosome-targeting antibiotics, which also bind in the NPET, specifically lincosamides and streptogramins B (hence this type of resistance is known as MLS_B)[17].

Significant efforts have been invested in developing newer generations of semi-synthetic macrolide antibiotics with improved binding properties, e.g. ketolides[2]. These drugs show improved activity against a variety of Gram-positive and Gram-negative pathogens, including those carrying inducible *erm* genes[3,18]. Nevertheless, bacteria that constitutively express Erm-methyltransferase enzymes that dimethylate A2058 still demonstrate high levels of resistance to all the known macrolide antibiotics[19,20]. Therefore, there is a pressing demand for the development of new macrolides active against Erm-modified ribosomes of resistant pathogens. Understanding at a structural level the detailed molecular mechanism of

Erm-mediated resistance to macrolides would provide key insights that are essential for the development of such compounds.

Previous attempts to explain the effect of A2058-methylation on drug binding were based on the structures of unmodified bacterial ribosomes complexed with various macrolides[21–24]. According to the prevailing *steric clash* model, the positions of the methyl group(s) added to the exocyclic N6 amino group of A2058 would overlap either with the 2′-hydroxyl group or the dimethyl-amino group of the desosamine sugar of a macrolide[21]. Due to this collision, the drug molecule should be unable to fully accommodate into its binding pocket and form hydrogen (H-) bond(s) with the A2058 and, therefore, cannot stably bind to the Erm-modified ribosome. However, the simplistic *steric clash* model is hard to be reconciled with the available experimental data. For instance, macrolide derivatives with 2′-deoxy or 3′-desmethyl desosamine, which were designed to reduce the steric clash with dimethylated A2058, were inactive against *Staphylococcus aureus* strains constitutively expressing Erm methyltransferase[25]. An alternative model is based on molecular dynamics simulation studies that suggest methylation of A2058 would result in complex structural rearrangements of the entire macrolide binding pocket, making drug binding impossible[26]. This model could rationalize the observed Erm-mediated resistance to all antibiotics of the MLS_B group, macrolides, lincosamides, and streptogramins B, which bind at the overlapping sites within the NPET of the bacterial ribosome. Although an attractive hypothesis, such structural rearrangements have never been experimentally verified or observed structurally.

By finding the conditions for expressing functionally-active Erm-methyltransferase in thermophilic bacterium *Thermus thermophilus* and solving the structures of the Erm-modified (A2058-dimethylated) and unmethylated 70S ribosome in complex with mRNA and aminoacylated tRNAs alone and in combination with macrolides, we demonstrate that neither of these models is likely to be correct. Instead, we present a principally new explanation of how A2058-dimethylation confers resistance to macrolide antibiotics. Not only we uncovered the mechanism of Erm-mediated macrolide resistance, but also our high-resolution structures of two macrolide antibiotics bound to the unmodified ribosome revealed a previously unknown role of the universal desosamine side chain in drug binding. The newly understood mode of interaction of this macrolide's moiety with the ribosome provides pivotal information for the design of macrolides that can overcome Erm-mediated resistance.

RESULTS

Engineering of Erm-expressing T. thermophilus strain.

Erm enzymes are expressed in a broad spectrum of pathogenic bacterial clinical isolates as well as in non-pathogenic native bacterial species where they produce strong resistance to macrolides[27]. The Erm methyltransferase operates during ribosome assembly because in the mature ribosome the target of Erm action, A2058 of the 23S rRNA, is inaccessible to the enzyme[28]. To obtain a structure of the Erm-modified ribosome, we have chosen the Gram-negative thermophilic bacterium *T. thermophilus* (*Tth*) as our experimental model because *Tth* ribosomes have been successfully used in the past for structure determination and

produce the highest-resolution data[29]. However, our attempts to express a functionally active Erm enzyme PikR2 from the mesophilic bacterium *Streptomyces venezuelae*[30] in this thermophilic host have failed, presumably due to protein instability at high growth temperature (Supplementary Table 1). To overcome this problem, we selected four *erm*-like genes from genomes of bacteria adapted for growth at elevated temperatures (Fig. 1b; Supplementary Figs. 1, 2; Supplementary Table 1). The genes were synthesized, cloned into the pBGAA1 vector[31], and expressed in *T. thermophilus* (Fig. 1c). Macrolide susceptibility testing of the plasmid-transformed *Tth* cells showed that the expression of an *erm*-like gene from *Bifidobacterium thermophilum* (referred hereafter as ErmBth) resulted in a strong resistance to the macrolide antibiotic erythromycin (ERY), increasing the minimal inhibitory concentration (MIC_{ERY}) for the ErmBth-expressing cells 1000-fold compared with the control cells carrying the empty vector (Supplementary Table 2).

To verify that the observed macrolide resistance results from the specific methyltransferase activity of ErmBth, we used a primer extension analysis to biochemically assess A2058 modification[32]. This method is based on the arrest of reverse transcriptase (RT) progression on the rRNA template due to its inability to incorporate a complementary nucleotide into the synthesized cDNA at the N6-dimethylated adenine. The expected cDNA arrest product of the RT reaction corresponding to the A2058 position was observed only on the 23S rRNA isolated from the *Tth* cells expressing ErmBth (Fig. 1d, lanes 2 and 3), confirming that ErmBth has the desired A2058-targeting methylation activity. Moreover, we found that the level of A2058-dimethylation can be significantly increased by growing the ErmBth-expressing cells in the presence of sub-inhibitory concentrations of ERY (Fig. 1d, e). By optimizing ERY concentration and growth temperature of the ErmBth-expressing *T. thermophilus* strain, we managed to reach the level of A2058 dimethylation as high as ~60% (Fig. 1e). Since X-ray crystallography is essentially an averaging technique, structural data could be confidently interpreted even if only half of the ribosomes are N6-dimethylated at A2058.

Structure of the 70S ribosome with m^6_2A2058.

We used our *T. thermophilus* strain expressing ErmBth-methyltransferase to purify 70S ribosomes for structural analysis. These were crystallized using previously published conditions[29] in a functional state that corresponds to a pre-peptide bond formation state of the ribosome, in which unreacted fMet-$tRNA_i^{Met}$ (in the form of its non-hydrolyzable analog fMet-NH-$tRNA_i^{Met}$) occupies the P-site, while non-hydrolyzable Phe-NH-$tRNA^{Phe}$ is bound to the A-site. By applying our recent improvements in complex preparation (see Materials and Methods), we were able to obtain crystal structures of the A2058-dimethylated and unmethylated *Tth* 70S ribosome in complex with mRNA and aminoacylated tRNAs determined at 2.4Å and 2.5Å resolution, respectively (Supplementary Table 3). For a more accurate understanding of drug-ribosome interactions, we determined structures of the unmethylated ribosomal functional complexes bound with two macrolide antibiotics, telithromycin (TEL) or erythromycin (ERY). These structures have been solved at 2.6Å and 2.55Å resolution, respectively, and represent the highest resolution 70S ribosome-macrolide structures available to date (Supplementary Table 3).

At this resolution, methylation of nucleotide bases can be directly visualized in the unbiased electron density maps (Fig. 2a, green mesh), and the N6-dimethylated A2058 (m^6_2A2058) can be confidently modeled in our structure (Fig. 2a, b; Extended Data Fig. 1a). Due to the presence of aminoacylated tRNAs (Extended Data Fig. 2), our structure of the WT ribosome with the unmodified A2058 reached a higher resolution than the previously reported structure[33], and clearly shows the position and orientation of the unmethylated A2058 residue which, therefore, serves as our reference point (Fig. 2c, d). Additional evidence for the presence of the methyl groups on m^6_2A2058 comes from the comparison of electron densities for the methylated m^6_2A2058 and the unmethylated A2057 in the 23S rRNA (negative control, Extended Data Fig. 1b) or the N6-dimethylated A1519 in the 16S rRNA (positive control, Extended Data Fig. 1c) of the same structure. In contrast to the predictions of MD simulations that A2058 modification would lead to a dramatic rearrangement of the macrolide binding site[26], no significant changes were observed in the orientations of the 23S rRNA nucleotides or the amino acid residues of the ribosomal proteins L4 and L22 neighboring A2058 in the ErmBth-modified ribosome (Fig. 3a, b). Most importantly, m^6_2A2058 appears in the same orientation relative to its neighbors as compared to the reference (unmodified) structure (Fig. 3c, d). Because A2058 methylation has been proposed to cause long-range structural rearrangements and affect the functionality of the ribosome[26], we also examined the ErmBth-modified ribosome for shifts in any of the key functional nucleotides around the PTC but failed to find any changes. Altogether our high-resolution structure of the A2058-dimethylated ribosome shows that the Erm-catalyzed rRNA modification does not cause any significant structural rearrangements in the macrolide binding site in the NPET.

Despite the fact that macrolide antibiotics have many H-bond donors and acceptors (Fig. 4a), there is only a single H-bond (between the 2′- OH of the desosamine sugar of a macrolide and the N1 atom of the A2058) that has been consistently observed in all previous structures of ribosome-bound macrolides (Fig. 4b)[21–24,34–36]. It has been suggested previously that the methyl groups of the N6-dimethylated A2058 residue can sterically clash with either the 2′-OH or the 3′-dimethyl-amino group of desosamine, leading to disruption of this critical H-bond and disturbing macrolide binding[21,22]. However, superposition of our structure of A2058-dimethylated *Tth* ribosome with that of the unmethylated *Tth* ribosome bound to ERY (or TEL) shows no overlap between the m^6_2A2058 methyl groups and the desosamine 2′-OH (Fig. 4b, c) or the desosamine dimethyl-amino groups (Fig. 4b, d). It is important to point out that, because the N6-nitrogen of the N6-dimethylated (and also N6-monomethylated) adenine residue has sp^2 geometry[37], the two methyl groups attached to the exocyclic amine of m^6_2A2058 are planar with the adenine heterocycle ring. Furthermore, the sp^2 geometry of the N6-atom does not allow free rotation around the C6-N6 bond in m^6_2A2058, excluding any alternative orientations of the methyl groups that could potentially result in a sterical clash with a macrolide. Thus, the analysis of the high-resolution structures of the ribosome-bound macrolides in complex with the unmodified ribosome and antibiotic-free A2058-dimethylated ribosome brings us to the conclusion that dimethylation of the exocyclic amine of A2058 by Erm methyltransferase does not result in a steric clash with desosamine sugar of the macrolide antibiotic or the loss of the H-bond between the

desosamine 2´-OH and the A2058 residue proposed previously to explain Erm-mediated resistance to macrolides.

Deciphering the role of desosamine in macrolide binding.

The dimethyl-amino group of desosamine has been shown previously to be crucial for the interaction of macrolides with the ribosome[38]. However, its exact role in drug binding has never been revealed. It is evident from the previous structural studies that no ribosomal component is directly involved in the interaction with this group. Moreover, by comparing all the available structures of ribosome-macrolide complexes, we noticed a significant variability in the orientation of this chemical group (Extended Data Figs. 3, 4), possibly due to varying interpretations of the electron density maps rather than differential placement of this chemical moiety. Notably, in none of the previous structures 3´-dimethyl-amino group of desosamine directly interacts with any of the ribosome counterparts.

In our 2.55Å and 2.6Å resolution structures of ribosome-bound ERY or TEL, both drug molecules are located in the canonical macrolide-binding pocket in the NPET near the PTC[23,24,35]. Interestingly, the shape of the electron density around the desosamine dimethyl-amino group clearly shows that the nitrogen lone pair of electrons (and this group as a whole) is pointed in the direction of A2058 (Fig. 5a, b, middle insets; Extended Data Fig. 5). This orientation is different from that in some of the previous structures, in which this group is oriented towards the exocyclic N6-amino group of the adjacent A2059 (Extended Data Fig. 4a,b)[22–24,34–36]. However, it resembles the orientation of this moiety in the 2.4Å-resolution structure of azithromycin bound to *Haloarcula marismortui* 50S ribosomal subunit (Extended Data Fig. 4c)[22] or the 3.0Å- resolution structure of this macrolide bound to *Tth* 70S ribosome (Extended Data Fig. 4d)[23].

Importantly, the high quality of the electron density maps of the new 70S-ERY and 70S-TEL structures allowed us to detect a distinct peak of positive electron density in close proximity to the dimethyl-amino moiety of desosamine in both complexes (Fig. 5a, b). We interpreted this electron density as a tightly coordinated water molecule based on the following criteria: (i) it fits snuggly between the two potential H-bond acceptors (nitrogen of the dimethyl-amino group of desosamine and one of the non-bridging oxygens of the G2505 phosphate) and a strong H-bond donor (exocyclic N6 amino group of the A2058); (ii) the distances between the aforementioned atoms and a putative water molecule in this location are all within the ideal range for H-bonds (2.5–3.5Å); (iii) the orientations of the proposed H-bonds correspond to the ideal tetrahedral geometry of the sp^3-hybridized oxygen atom of a water molecule (Fig. 5a, b); (iv) ideal planar geometry with the heterocycle ring for the H-bond from the A2058 N6 donor to the oxygen acceptor of the modeled water (Fig. 5a, b, middle insets); (v) the observed electron density is too weak to be attributed to more electron-dense ions, such as Mg^{2+} or K^+. Thus, because of the high resolution of our new 70S-ERY and 70S-TEL structures, it becomes evident that the high affinity of desosamine-containing macrolides to the ribosome is mediated by a strong H-bond mediated by the water molecule, which in turn is tightly coordinated by the exocyclic N6-amino group of A2058 and the phosphate of G2505 of 23S rRNA (Fig. 5c). This critical, water-mediated contact between a macrolide molecule and the ribosome, which has never been reported before, illuminates the

previously obscure role of the dimethyl-amino moiety of desosamine in macrolide binding to the ribosome. Consistent with our observations, re-evaluation of the electron density maps of previously published ribosome-macrolide complex structures revealed the presence of this same water molecule; a peak of positive electron density can be seen in the same location in all structures with resolution ≤ 2.7Å[22,34]. However, it is the high quality of our structural data, which allows for interpretation of this density peak as a water molecule and reveals the possibly critical role of this, previously overlooked, player in macrolide binding.

Structural basis for Erm-mediated macrolide resistance.

The discovery of a key water molecule that mediates macrolide binding to the ribosome and the solved structure of the A2058-dimethylated ribosome allows a conceptually new rationalization of Erm-mediated macrolide resistance in molecular terms. In the unmethylated ribosome, the N6-amino group of the A2058 residue serves as an H-bond donor that shares one proton with the H_2O oxygen atom (Fig. 5c, e). This water molecule, in turn, shares one of its protons with the G2505 phosphate and the other proton with the dimethyl-amino group of a macrolide. Dimethylation (but not monomethylation) of the N6-amino group of the A2058 by Erm-methyltransferases makes coordination of this water molecule impossible due to the inability of the A2058 dimethyl-amino group to serve as a proton donor. Furthermore, one of the $m^6{}_2$A2058 methyl groups would physically displace the water molecule (Fig. 5d, e), leaving the dimethyl-amine of desosamine without the mediator of its interaction with the G2505 phosphate. The lack of such interaction in the A2058-dimethylated ribosome would have a strong negative effect on the free energy of the drug-ribosome complex leading to macrolide resistance. The same water molecule could also be observed in the current structure of wild-type ribosome in the absence of a macrolide. Therefore, it is conceivable that it could be important for normal ribosome functioning by stabilizing the local structure of the 23S rRNA. Displacement of this water molecule by dimethylation of A2058 and the resulting alteration in the local 23S rRNA structure and/or the chemical makeup of the NPET could potentially account for reduced fitness of cells expressing Erm methyltransferase, linked to aberrant translation of specific proteins[39].

Besides the Erm-catalyzed dimethylation of A2058, mutations of this nucleotide to guanine, cytosine, or uracyl also result in macrolide resistance[40,41]. The discovered water-mediated interaction of macrolides with the ribosome allows re-evaluation of the mechanism of antibiotic resistance caused by these mutations (Extended Data Fig. 6a). *In silico* modeling of the A2058 mutations reveals that pyrimidine bases at this position would be placed too far from the desosamine moiety of a macrolide to establish any interactions with the drug (including water-mediated contacts) (Extended Data Fig. 6c, d). Replacing A2058 with guanine was proposed to lead to a steric clash with the C4 carbon of the macrolactone ring (Extended Data Fig. 6b)[22]. Our structures show that in addition to this mechanism, G2058 would not be able to coordinate the critical molecule of water the same way as adenine because the O6 atom of guanine cannot serve as an H-bond donor (Extended Data Fig. 6b).

Erm-mediated dimethylation of A2058 residue is the major clinical mechanism of bacterial resistance not only to macrolides but also to lincosamides and type B streptogramins.

Comparison of our structure of the A2058-dimethylated 70S ribosome with the previously reported structure of the ribosome-bound lincosamide antibiotic clindamycin[24] reveals a significant steric clash between one of the methyl groups of $m^6{}_2$A2058 and the 2´- and 3´-OH groups of the 7-chloro-1-methylthio-lincosamine moiety of the drug (Extended Data Fig. 7a, b). In contrast to macrolides and type B streptogramins, a similar high level of resistance to lincosamides could be achieved not only by dimethylation but also by monomethylation of A2058[27,42]. Due to the sp^2 geometry of the N6-atom, the single methyl group of the monomethylated A2058 residue can exist in two alternative conformations: *syn*-methyl (with the methyl group oriented towards the Watson-Crick edge of the nucleotide) and *anti*-methyl (with the methyl group rotated towards the N7-atom of the adenine base)[43]. Importantly, it is only the *syn*-methyl conformation of the N6-methyl group of monomethylated A2058 that would clash with the ribosome-bound lincosamide drug, whereas the N6-methyl group in the *anti*-methyl conformation not only avoids the clash but could also retain all H-bonding capabilities potentially critical for the lincosamide drug binding (Extended Data Fig. 7b). However, because of a steric hindrance from the N7-atom of adenine, the *syn-methyl* conformation is energetically more favorable than the *anti*-methyl conformation[43]. Unlike macrolides, lincosamides, whose binding to the ribosome is characterized by 3-order of magnitude lower affinity[44,45], apparently cannot overcome the energy needed to re-orient the methyl group of N6-monomethylated A2058 into unfavorable *anti*-methyl conformation. Thus, N6-monomethylation of the A2058 is likely to cause resistance to lincosamides via the same steric hindrance mechanism as the dimethylation of the same adenine residue (Extended Data Fig. 7a, b).

Interestingly, similar superpositioning of the structure of the A2058-dimethylated ribosome with the published structure of type B streptogramin antibiotic quinupristin complexed to the ribosome[46] does not show any overlap between $m^6{}_2$A2058 and the drug (Extended Data Fig. 7c, d). Moreover, the N6-dimethyl is located on the opposite side of the A2058 nucleotide relative to the closest dimethyl-amino-phenylalanine moiety of the ribosome-bound quinupristin (Extended Data Fig. 7d). This moiety likely forms a Van-der-Waals contact with the N3 atom of the A2058 residue. However, because the A2058 nucleotides in the two superimposed structures have the same conformations, the N6-dimethylation of A2058 is unlikely to perturb this contact (Extended Data Fig. 7d). Overall, structural analysis shown in Extended Data Fig. 7c does not reveal disruptions of any critical contacts of the drug with the ribosome that could be caused by Erm-catalyzed A2058 dimethylation and, thus, does not offer a straightforward explanation for the molecular mechanism of the Erm-mediated streptogramin B resistance, which still remains enigmatic. Although Erm-mediated dimethylation of A2058 renders bacterial ribosomes resistant to macrolides, lincosamides, and streptogramins B, the actual mechanism of resistance at a molecular level appears to be different for each class of NPET-targeting antibiotics.

DISCUSSION

Our work was motivated by the lack of understanding of why Erm-mediated dimethylation of the 23S rRNA residue A2058, located in the macrolide binding site, confers resistance to macrolide antibiotics. The high-resolution structures of two macrolides bound to the sensitive ribosomes and the first structure of the A2058-dimethylated 70S ribosome

provided critical clues that allowed us to propose a model that offers a likely explanation of how this mechanism of resistance actually operates. The discovery of a previously cryptic water molecule that appears to be playing a pivotal role in macrolide binding clarified the importance of interactions of the desosamine group of the drug with the ribosomal target. The other key breakthrough came from optimizing the expression of Erm-methyltransferase encoded in the genome of a moderate bacterial thermophile *B. thermophilum* in the highly thermophilic bacterial host *T. thermophilus*. This permitted us to prepare the crystallizable 70S ribosomes with a highly methylated A2058 residue. The revealed placement of methyl groups appended to the exocyclic N6-amino group of A2058 showed that the water-mediated bridging becomes impossible in the Erm-modified ribosome, which likely leads to the reduced affinity of the macrolide drugs that rely on this contact.

Altogether, our structural study uncovering the molecular mechanism of Erm-mediated resistance could be a starting point for the rational knowledge-based development of new MLS_B antibiotics active against challenging drug-resistant pathogens. This quest will be likely additionally stimulated by the recently discovered new combinatorial approaches for the synthesis of novel macrolides[47], streptogramins[48], and other drugs. Interestingly, all previous attempts to make macrolides active against Erm-modified ribosomes relied on derivatization of the existing macrolides to provide additional anchoring points that improved their overall affinity[49]. However, none of the derivatizations affected the desosamine likely due to its importance in overall drug binding. Unfortunately, the affinities of the resulting semi-synthetic macrolides of a newer generation (such as telithromycin or solithromycin) to the modified ribosome are too low to allow using these drugs for the treatment of infections caused by pathogens with expressed *erm* genes[2,19,50]. Now, when the precise role of the desosamine sugar in macrolide binding to the ribosome is uncovered, this information may become instrumental in the designing of macrolides that can overcome Erm-mediated resistance.

Extended Data

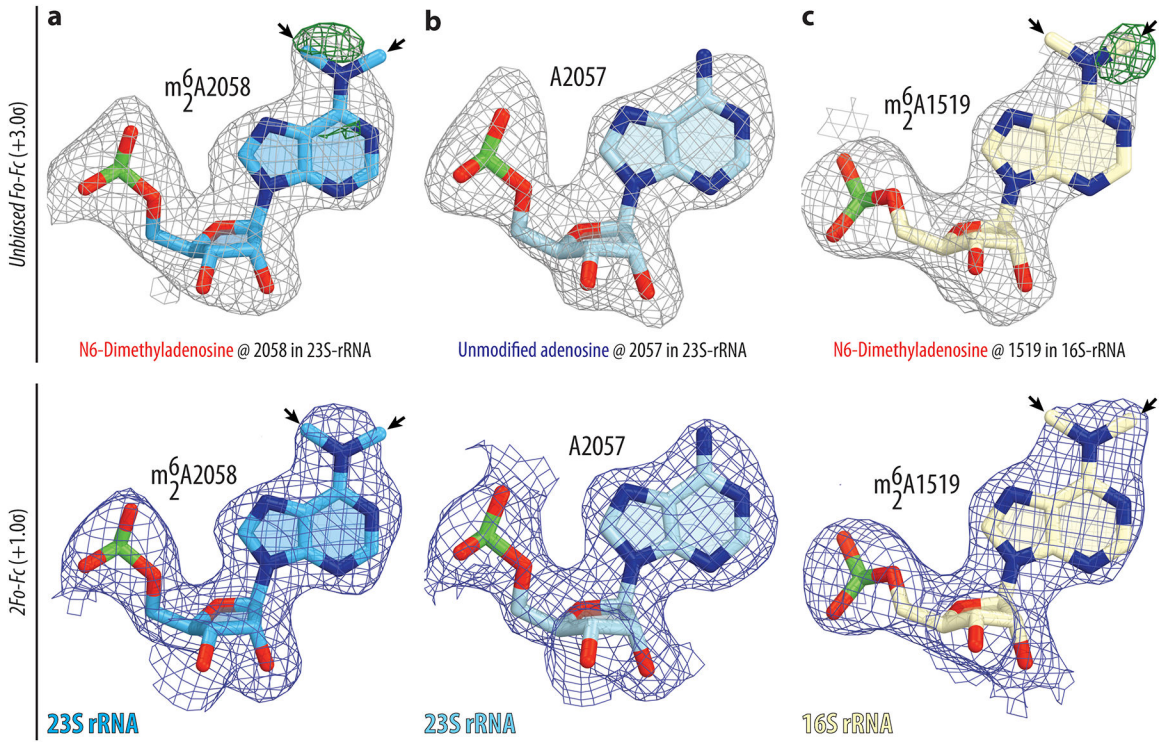

Extended Data Fig. 1. Electron density maps of N6-dimethylated and unmethylated adenine residues in the current structure of the A2058-methylated *Thermus thermophilus* 70S ribosome.

(**a, b, c**) Unbiased F_o-F_c (top row; grey and green mesh) and $2F_o$-F_c (bottom row; blue mesh) electron density maps corresponding to the (**a**) N6-dimethylated A2058 residue, or (**b**) the unmethylated A2057 residue of the 23S rRNA, or (**c**) N6-dimethylated A1519 residue of the 16S rRNA (naturally modified by methyltransferase KsgA) in the *T. thermophilus* 70S ribosome contoured at 3.0σ and 1.0σ, respectively. The refined models are displayed in the corresponding electron density maps. Carbon atoms are colored blue for the methylated A2058, light blue for the unmethylated A2058, and pale yellow for the methylated A1519. Nitrogens are colored dark blue; oxygens are red, phosphorus atoms are green. Grey mesh shows the F_o-F_c map after refinement with the entire modified nucleotide omitted. Green mesh shows the F_o-F_c electron density map after refinement with the nucleotides A2058 and A1519 built as regular unmethylated adenines. We show electron density maps for the A2057 and the A1519 nucleotides as negative and positive control references originating from the same structure.

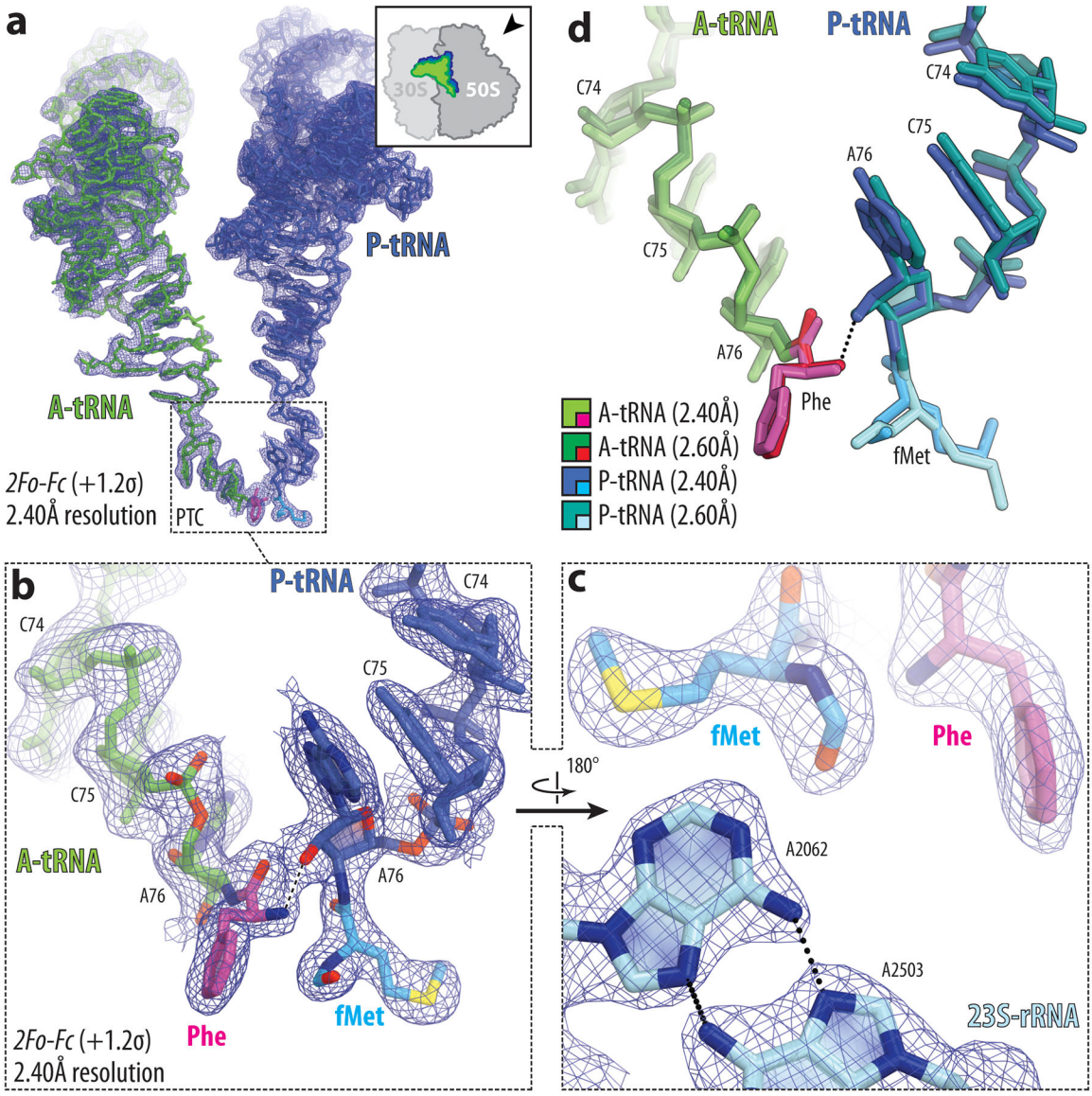

Extended Data Fig. 2. Aminoacylated A- and P-site tRNAs bound to the A2058-methylated 70S ribosome.

(**a, b, c**) High-resolution (2.4Å) *2Fo-Fc* electron density map (blue mesh) for the ribosome-bound A-site Phe-NH-tRNA^{Phe} (green) and the P-site fMet-NH-tRNA$_i^{Met}$ (dark blue). The refined models of tRNAs are displayed in their respective electron density map contoured at 1.2σ. (**a**) The entire bodies of the A- and P-site tRNAs viewed from the back of the 50S subunit, as indicated by the inset. Ribosome subunits are omitted for clarity. (**b, c**) Close-up views of the tRNA CCA-ends carrying phenylalanyl (magenta) and formyl-methionyl (blue) moieties. Nitrogens are colored blue; oxygens are red, sulfur is yellow. In (B), H-bond between the α-amino group and the 2'-OH of the A76 of the P-site tRNA is shown with the black dotted line. This H-bond is pivotal to optimally orient α-amine for an in-line nucleophilic attack onto the carbonyl carbon of the P-site substrate. (**d**) Superimposed models of aminoacylated tRNAs from the current 2.4Å structure of A2058-methylate 70S

ribosome with the previous 2.6Å structure of A2058-unmethylated ribosome (PDB entry 1VY4[33]).

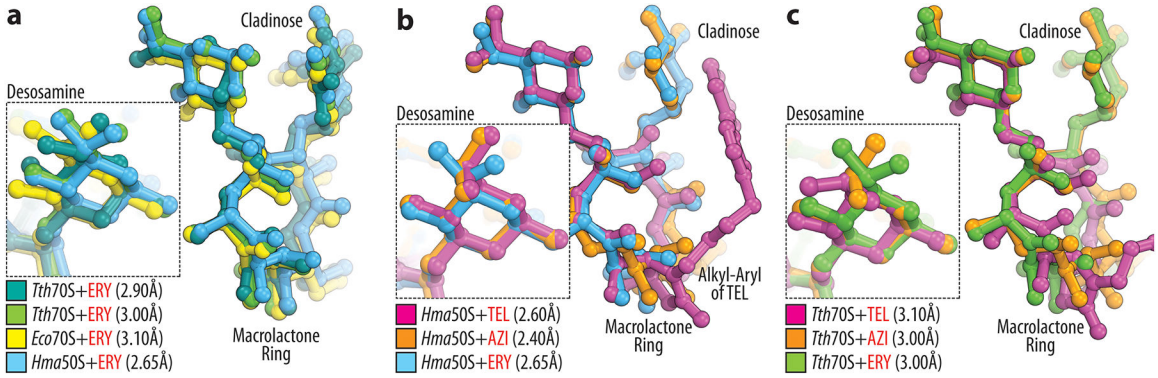

Extended Data Fig. 3. Structural comparison of the ribosome-bound macrolides.

(**a**) Superpositioning of the structures of ERY in complex with the 70S ribosomes from *T. thermophilus* (teal, PDB entry 6ND6[35]; green, PDB entry 4V7X[23]), *E. coli* (yellow, PDB entry 4V7U[24]), or *H. marismortui* (blue, PDB entry 1YI2[22]). (**b**) Superpositioning of the structures of the 50S ribosomal subunit from *H. marismortui* in complex with ERY (blue, PDB entry 1YI2[22]), azithromycin (AZI, orange, PDB entry 1YHQ[22]), and telithromycin (TEL, magenta, PDB entry 1YIJ[22]). (**c**) Superpositioning of the structures of the 70S ribosome from *T. thermophilus* in complex with ERY (green, PDB entry 4V7X[23]), azithromycin (AZI, orange, PDB entry 4V7Y[23]), and telithromycin (TEL, magenta, PDB entry 4V7Z[23]). The insets show closed up views of the desosamine sugar. Note a significant variability in the orientation of the dimethylamino groups of the desoamine sugar among ribosome-bound macrolides.

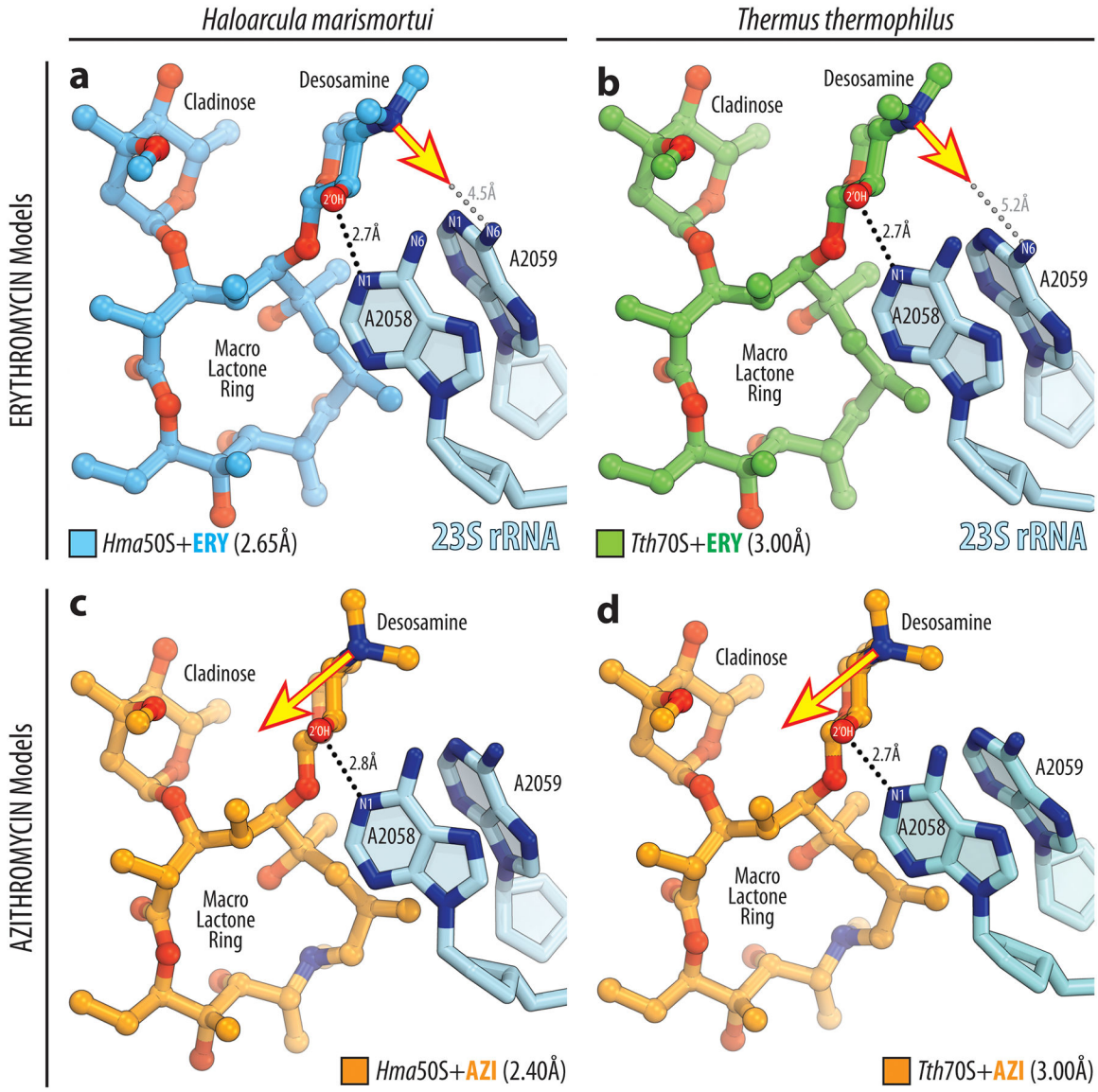

Extended Data Fig. 4. Analysis of the orientation of the dimethyl-amino group in previously published structures of ribosome-bound macrolides.

a, b) In the structures of erythromycin (ERY) in complex with *H. marismortui* 50S subunit (blue, PDB entry 1YI2[22]), or *T. thermophilus* 70S ribosome (green, PDB entry 4V7X[23]) the nitrogen lone pair of electrons on the dimethyl-amino group of the desosamine sugar is oriented towards the exocyclic N6-amino group of the A2059 nucleotide of the 23S rRNA (blue), as indicated by the yellow arrow. Note that the formation of a direct H-bond, in this case, is impossible due to the large distance between the potential interacting partners (grey dashed lines). H-bond between 2'-OH group of desosamine sugar and N1 atom of A2058 is shown by the black dashed lines. (**c, d**) In the structures of azithromycin (AZI) in complex with *H. marismortui* 50S subunit (orange, PDB entry 1YHQ[22]), or *T. thermophilus* 70S ribosome (orange, PDB entry 4V7Y[23]) the nitrogen lone pair of electrons of the dimethyl-amino group on the desosamine is rotated by approximately 90 degrees away from the

residue A2059 in the direction of residue A2058, as indicated by the yellow arrow. Note that, in this case, there are no obvious binding partners for this group on the ribosome.

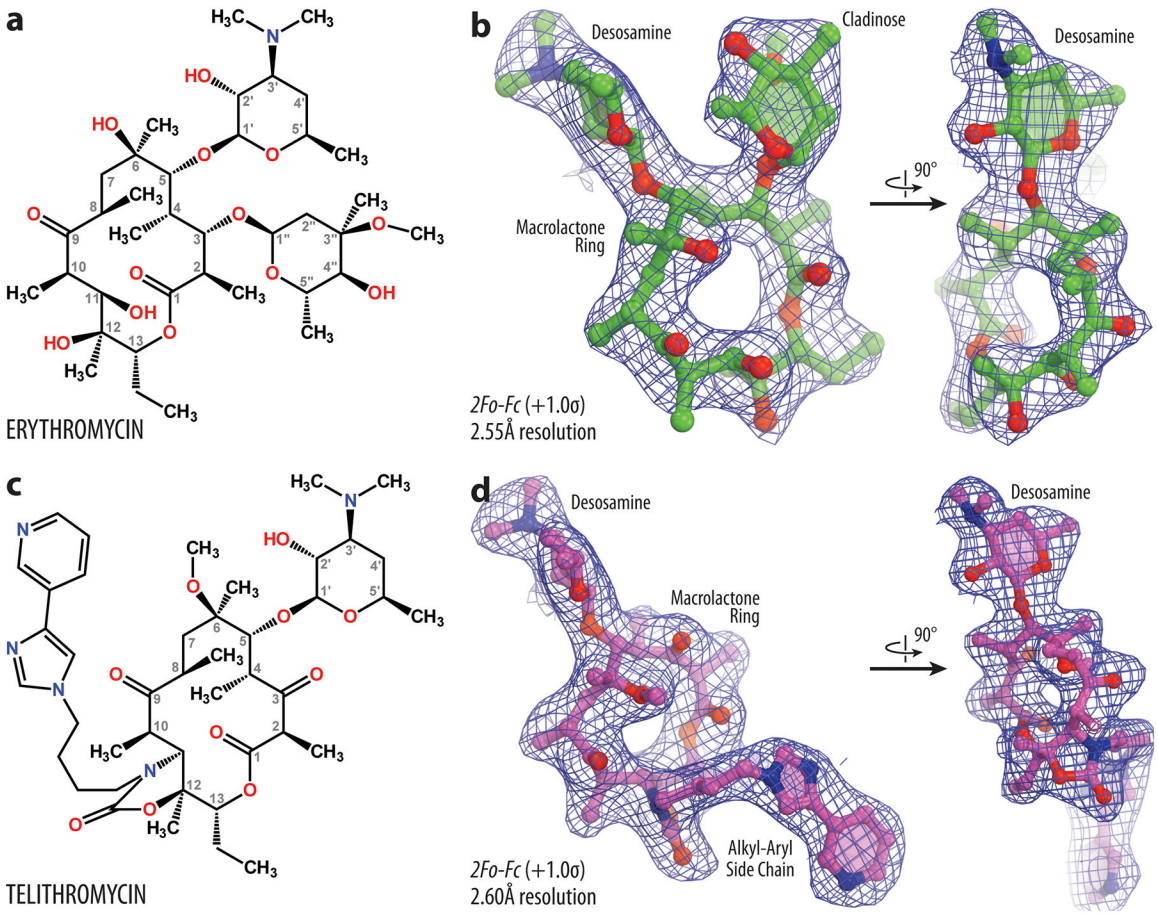

Extended Data Fig. 5. Electron density maps of ribosome-bound erythromycin and telithromycin.

(**a, c**) Chemical structures of NPET-binding macrolide antibiotics erythromycin (a, ERY) and telithromycin (c, TEL). (**b, d**) High-resolution $2F_o$-F_c electron density maps (blue mesh) of ERY (b, green) and TEL (d, magenta) in complex with the *T. thermophilus* 70S ribosome viewed from two different perspectives. The refined models of ERY or TEL are displayed in their respective electron densities contoured at 1.0σ. Nitrogen atoms are colored blue; oxygens are red. Key chemical moieties of each drug are labeled.

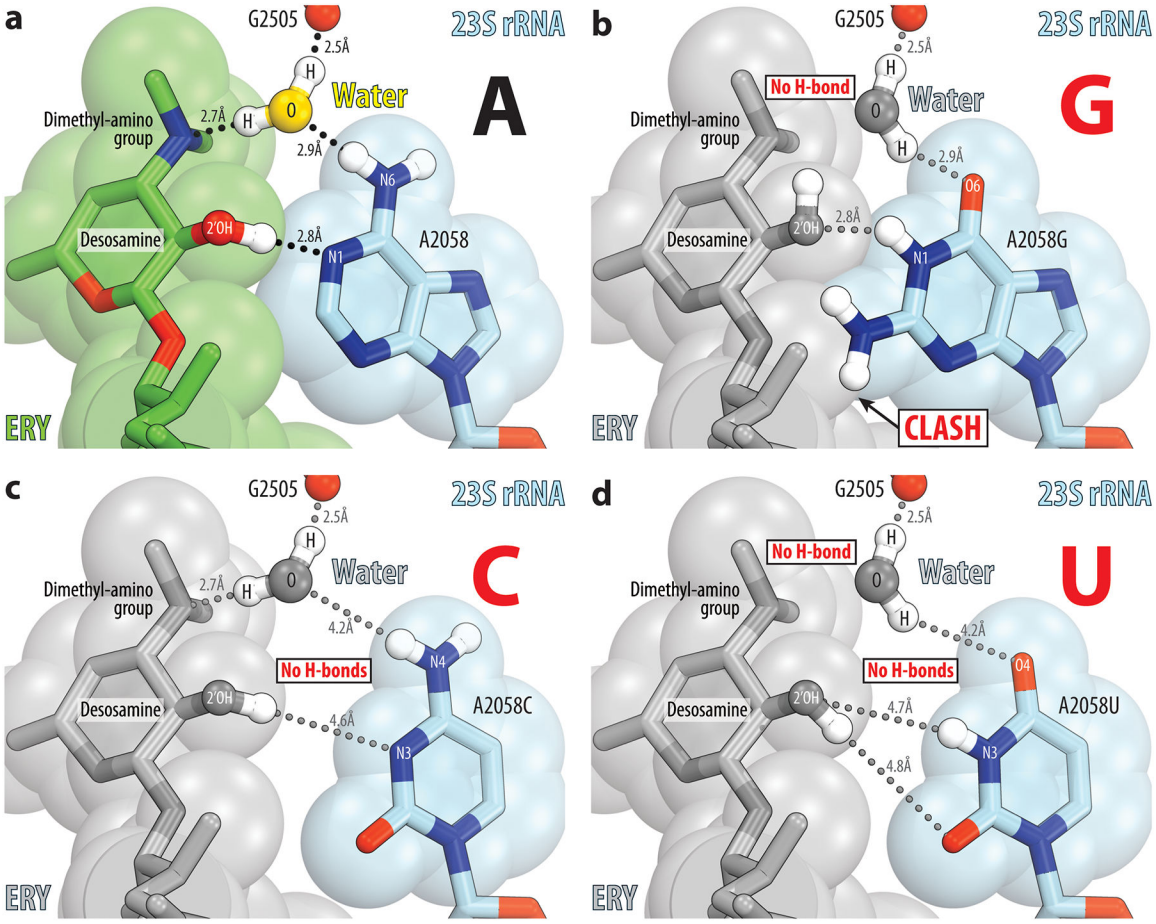

Extended Data Fig. 6. *In silico* modeling of the A2058 mutants.

(**a**) Water-mediated coordination of a macrolide antibiotic (ERY, green) by the wild-type A2058 nucleotide (blue) of the 23S rRNA. Existing H-bonds are shown by the black dashed lines. (**b, c, d**) Strong water-mediated coordination of a macrolide molecule on the ribosome becomes impossible when the adenine nucleotide at position 2058 of the 23S rRNA is mutated to guanine (b), cytosine (c), or uracil (d) nucleotides. Non-existing H-bonds (due to distance restraints) are shown by the grey dashed lines. Note that in the case of A2058G mutation, in addition to the inability of the guanine nucleotide to coordinate a macrolide via a water molecule, the exocyclic N2-amino group of guanine clashes with the C4-methyl group attached to the macrolactone ring of a macrolide molecule.

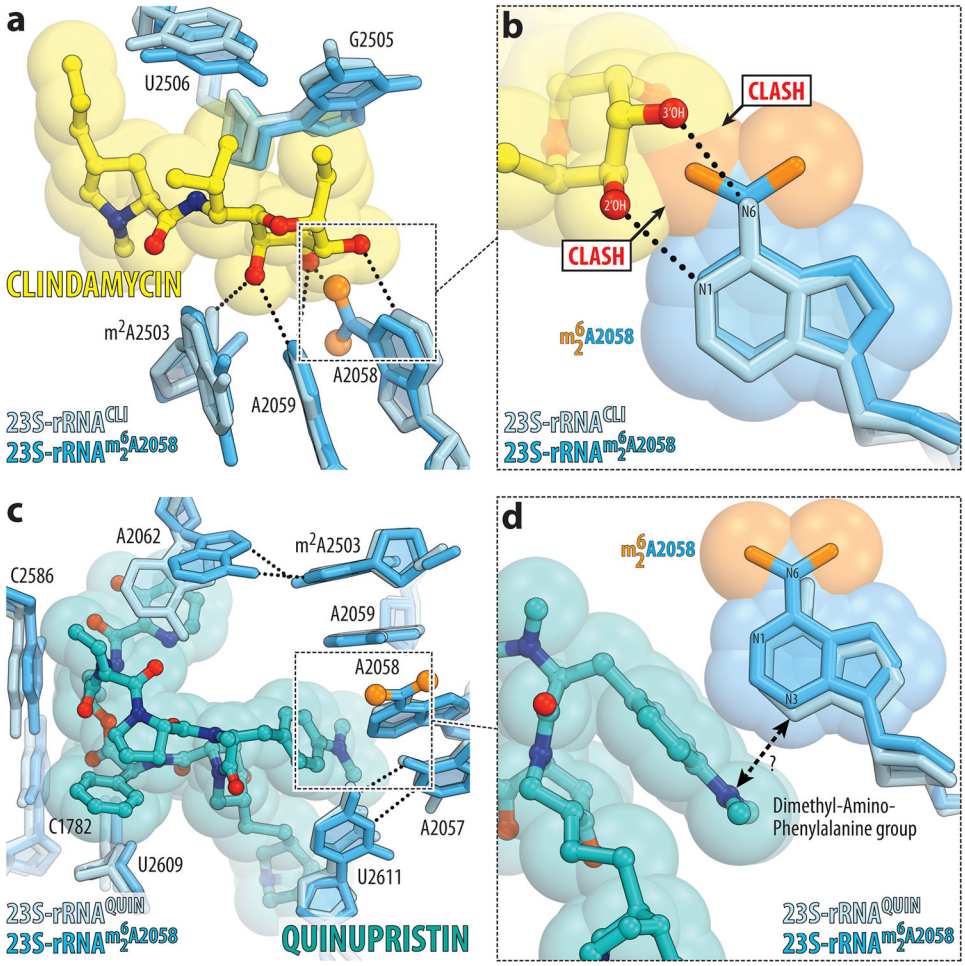

Extended Data Fig. 7. Alignment of the structures of A2058-methylated 70S ribosome with the ribosome-bound clindamycin or quinupristin.

Superposition of the current structure of A2058-methylated 70S ribosome with the structure of ribosome-bound lincosamide antibiotic clindamycin (yellow, PDB entry 4V7V[24]) (**a, b**) or streptogramin type B antibiotic quinupristin (teal, PDB entry 4U26[46]) (**c, d**). Nucleotides of the Erm-modified and unmodified ribosomes are shown in blue and light blue, respectively. Methylated A2058 residue is shown in blue with the methyl groups highlighted in orange. All structures were aligned based on domain V of the 23S rRNA.

Supplementary Material

Refer to Web version on PubMed Central for supplementary material.

ACKNOWLEDGMENTS

We thank Dr. Nora Vazquez-Laslop for valuable discussions and critical feedback and all members of A.S.M. and Y.S.P. laboratories for valuable suggestions. We thank the staff at NE-CAT beamlines 24ID-C and 24ID-E for help with data collection and freezing of the crystals, especially Drs. Malcolm Capel, Frank Murphy, Igor Kourinov, Anthony Lynch, Surajit Banerjee, David Neau, Jonathan Schuermann, Narayanasami Sukumar, James Withrow, Kay Perry, and Cyndi Salbego.

This work is based upon research conducted at the Northeastern Collaborative Access Team beamlines, which are funded by the National Institute of General Medical Sciences from the National Institutes of Health [P30-GM124165 to NE-CAT]. The Eiger 16M detector on 24-ID-E beamline is funded by a NIH-ORIP HEI grant [S10-OD021527 to NE-CAT]. This research used resources of the Advanced Photon Source, a U.S. Department of Energy (DOE) Office of Science User Facility operated for the DOE Office of Science by Argonne National Laboratory under Contract No. DE-AC02-06CH11357.

This work was supported by Illinois State startup funds [to Y.S.P.], National Institutes of Health [R21-AI137584 to A.S.M. and Y.S.P.; R01-GM132302 to Y.S.P.; R35-GM127134 to A.S.M.; R01-GM094157 to S.T.G.], USDA National Insititute for Food and Agriculture [Hatch Project 1016013 to S.T.G.], Swedish Research Council (Vetenskapsrådet) [2015-04746 and 2019-01085 to G.C.A].

REFERENCES FOR THE MAIN TEXT

1. Wilson DN Ribosome-targeting antibiotics and mechanisms of bacterial resistance. Nat. Rev. Microbiol 12, 35–48 (2014). [PubMed: 24336183]
2. Fernandes P, Martens E, Bertrand D & Pereira D The solithromycin journey-It is all in the chemistry. Bioorg. Med. Chem 24, 6420–6428 (2016). [PubMed: 27595539]
3. Dinos GP The macrolide antibiotic renaissance. Br. J. Pharmacol 174, 2967–2983 (2017). [PubMed: 28664582]
4. Vazquez-Laslop N & Mankin AS How macrolide antibiotics work. Trends Biochem. Sci 43, 668–684 (2018). [PubMed: 30054232]
5. Nunez-Samudio V & Chesneau O Functional interplay between the ATP binding cassette Msr(D) protein and the membrane facilitator superfamily Mef(E) transporter for macrolide resistance in *Escherichia coli*. Res. Microbiol 164, 226–235 (2013). [PubMed: 23261969]
6. Fyfe C, Grossman TH, Kerstein K & Sutcliffe J Resistance to macrolide antibiotics in public health pathogens. Cold Spring Harb. Perspect. Med 6, a025395 (2016). [PubMed: 27527699]
7. Morar M, Pengelly K, Koteva K & Wright GD Mechanism and diversity of the erythromycin esterase family of enzymes. Biochemistry 51, 1740–1751 (2012). [PubMed: 22303981]
8. Shakya T & Wright GD Nucleotide selectivity of antibiotic kinases. Antimicrob. Agents Chemother 54, 1909–1913 (2010). [PubMed: 20231391]
9. Poehlsgaard J & Douthwaite S Macrolide antibiotic interaction and resistance on the bacterial ribosome. Curr. Opin. Investig. Drugs 4, 140–148 (2003).
10. Sutcliffe J & Leclercq R Mechanisms of resistance to macrolides, lincosamides, and ketolides. in Macrolide Antibiotics (eds. Schönfeld W & Kirst HA) 281–318 (Birkhäuser Verlag, Basel, 2002).
11. Roberts MC et al. Nomenclature for macrolide and macrolide-lincosamide-streptogramin B resistance determinants. Antimicrob. Agents Chemother 43, 2823–2830 (1999). [PubMed: 10582867]
12. Skinner R, Cundliffe E & Schmidt FJ Site of action of a ribosomal RNA methylase responsible for resistance to erythromycin and other antibiotics. J. Biol. Chem 258, 12702–12706 (1983). [PubMed: 6195156]
13. Uchiyama H & Weisblum B N-Methyl transferase of *Streptomyces erythraeus* that confers resistance to the macrolide-lincosamide-streptogramin B antibiotics: amino acid sequence and its homology to cognate R-factor enzymes from pathogenic bacilli and cocci. Gene 38, 103–110 (1985). [PubMed: 3934045]
14. Arthur M, Brisson-Noel A & Courvalin P Origin and evolution of genes specifying resistance to macrolide, lincosamide and streptogramin antibiotics: data and hypotheses. J. Antimicrob. Chemother 20, 783–802 (1987). [PubMed: 3326871]
15. Lai CJ & Weisblum B Altered methylation of ribosomal RNA in an erythromycin-resistant strain of *Staphylococcus aureus*. Proc. Natl. Acad. Sci. USA 68, 856–860 (1971). [PubMed: 5279527]
16. Goldman RC & Kadam SK Binding of novel macrolide structures to macrolides-lincosamides-streptogramin B-resistant ribosomes inhibits protein synthesis and bacterial growth. Antimicrob. Agents Chemother 33, 1058–1066 (1989). [PubMed: 2506804]
17. Vester B & Douthwaite S Macrolide resistance conferred by base substitutions in 23S rRNA. Antimicrob. Agents Chemother 45, 1–12 (2001). [PubMed: 11120937]

18. Farrell DJ, Mendes RE & Jones RN Antimicrobial activity of solithromycin against serotyped macrolide-resistant *Streptococcus pneumoniae* isolates collected from U.S. medical centers in 2012. Antimicrob. Agents Chemother 59, 2432–2434 (2015). [PubMed: 25605359]
19. Liu M & Douthwaite S Activity of the ketolide telithromycin is refractory to Erm monomethylation of bacterial rRNA. Antimicrob. Agents Chemother 46, 1629–1633 (2002). [PubMed: 12019067]
20. Liu M & Douthwaite S Resistance to the macrolide antibiotic tylosin is conferred by single methylations at 23S rRNA nucleotides G748 and A2058 acting in synergy. Proc. Natl. Acad. Sci. USA 99, 14658–14663 (2002). [PubMed: 12417742]
21. Hansen JL et al. The structures of four macrolide antibiotics bound to the large ribosomal subunit. Mol. Cell 10, 117–128 (2002). [PubMed: 12150912]
22. Tu D, Blaha G, Moore PB & Steitz TA Structures of MLSBK antibiotics bound to mutated large ribosomal subunits provide a structural explanation for resistance. Cell 121, 257–270 (2005). [PubMed: 15851032]
23. Bulkley D, Innis CA, Blaha G & Steitz TA Revisiting the structures of several antibiotics bound to the bacterial ribosome. Proc. Natl. Acad. Sci. USA 107, 17158–17163 (2010). [PubMed: 20876130]
24. Dunkle JA, Xiong L, Mankin AS & Cate JH Structures of the Escherichia coli ribosome with antibiotics bound near the peptidyl transferase center explain spectra of drug action. Proc. Natl. Acad. Sci. USA 107, 17152–17157 (2010). [PubMed: 20876128]
25. LeTourneau N, Vimal P, Klepacki D, Mankin A & Melman A Synthesis and antibacterial activity of desosamine-modified macrolide derivatives. Bioorg. Med. Chem. Lett 22, 4575–4578 (2012). [PubMed: 22738632]
26. Small MC, Lopes P, Andrade RB & Mackerell AD Jr. Impact of ribosomal modification on the binding of the antibiotic telithromycin using a combined grand canonical monte carlo/molecular dynamics simulation approach. PLoS Comput. Biol 9, e1003113 (2013). [PubMed: 23785274]
27. Weisblum B Erythromycin resistance by ribosome modification. Antimicrob. Agents Chemother 39, 577–585 (1995). [PubMed: 7793855]
28. Pokkunuri I & Champney WS Characteristics of a 50S ribosomal subunit precursor particle as a substrate for ermE methyltransferase activity and erythromycin binding in *Staphylococcus aureus*. RNA Biol. 4, 147–153 (2007). [PubMed: 18094627]
29. Polikanov YS, Melnikov SV, Soll D & Steitz TA Structural insights into the role of rRNA modifications in protein synthesis and ribosome assembly. Nat. Struct. Mol. Biol 22, 342–344 (2015). [PubMed: 25775268]
30. Almutairi MM et al. Resistance to ketolide antibiotics by coordinated expression of rRNA methyltransferases in a bacterial producer of natural ketolides. Proc. Natl. Acad. Sci. USA 112, 12956–12961 (2015). [PubMed: 26438831]
31. Carr JF, Danziger ME, Huang AL, Dahlberg AE & Gregory ST Engineering the genome of *Thermus thermophilus* using a counterselectable marker. J. Bacteriol 197, 1135–1144 (2015). [PubMed: 25605305]
32. Bailey M, Chettiath T & Mankin AS Induction of erm(C) expression by noninducing antibiotics. Antimicrob. Agents Chemother. 52, 866–874 (2008).
33. Polikanov YS, Steitz TA & Innis CA A proton wire to couple aminoacyl-tRNA accommodation and peptide-bond formation on the ribosome. Nat. Struct. Mol. Biol 21, 787–793 (2014). [PubMed: 25132179]
34. Almutairi MM et al. Co-produced natural ketolides methymycin and pikromycin inhibit bacterial growth by preventing synthesis of a limited number of proteins. Nucleic Acids Res. 45, 9573–9582 (2017). [PubMed: 28934499]
35. Svetlov MS et al. High-resolution crystal structures of ribosome-bound chloramphenicol and erythromycin provide the ultimate basis for their competition. RNA 25, 600–606 (2019). [PubMed: 30733327]
36. Khabibullina NF et al. Structure of dirithromycin bound to the bacterial ribosome suggests new ways for rational improvement of macrolides. Antimicrob. Agents Chemother 63, e02266–18 (2019). [PubMed: 30936109]

37. Zhang Y, El Kouni MH & Ealick SE Substrate analogs induce an intermediate conformational change in *Toxoplasma gondii* adenosine kinase. Acta Crystallogr. D Biol. Crystallogr 63, 126–134 (2007). [PubMed: 17242506]
38. Pestka S & Lemahieu RA Effect of erythromycin analogues on binding of [^{14}C]erythromycin to *Escherichia coli* ribosomes. Antimicrob. Agents Chemother 6, 479–488 (1974). [PubMed: 4157349]
39. Gupta P, Sothiselvam S, Vazquez-Laslop N & Mankin AS Deregulation of translation due to post-transcriptional modification of rRNA explains why erm genes are inducible. Nat. Commun 4, 1984 (2013). [PubMed: 23749080]
40. Douthwaite S & Aagaard C Erythromycin binding is reduced in ribosomes with conformational alterations in the 23 S rRNA peptidyl transferase loop. J. Mol. Biol 232, 725–731 (1993). [PubMed: 7689111]
41. Pfister P et al. The structural basis of macrolide-ribosome binding assessed using mutagenesis of 23S rRNA positions 2058 and 2059. J. Mol. Biol 342, 1569–1581 (2004). [PubMed: 15364582]
42. Calcutt MJ & Cundliffe E Cloning of a lincosamide resistance determinant from *Streptomyces caelestis*, the producer of celesticetin, and characterization of the resistance mechanism. J. Bacteriol 172, 4710–4714 (1990). [PubMed: 2376570]
43. Roost C et al. Structure and thermodynamics of N6-methyladenosine in RNA: a spring-loaded base modification. J. Am. Chem. Soc 137, 2107–2115 (2015). [PubMed: 25611135]
44. Contreras A & Vazquez D Cooperative and antagonistic interactions of peptidyl-tRNA and antibiotics with bacterial ribosomes. Eur. J. Biochem 74, 539–547 (1977). [PubMed: 323015]
45. Pestka S Binding of [^{14}C]erythromycin to *Escherichia coli* ribosomes. Antimicrob. Agents Chemother 6, 474–478 (1974). [PubMed: 4157348]
46. Noeske J et al. Synergy of streptogramin antibiotics occurs independently of their effects on translation. Antimicrob. Agents Chemother 58, 5269–5279 (2014). [PubMed: 24957822]
47. Seiple IB et al. A platform for the discovery of new macrolide antibiotics. Nature 533, 338–345 (2016). [PubMed: 27193679]
48. Li Q et al. Synthetic group A streptogramin antibiotics that overcome Vat resistance. Nature 586, 145–150 (2020). [PubMed: 32968273]
49. Hansen LH, Mauvais P & Douthwaite S The macrolide-ketolide antibiotic binding site is formed by structures in domains II and V of 23S ribosomal RNA. Mol. Microbiol 31, 623–631 (1999). [PubMed: 10027978]
50. Scheinfeld N Telithromycin: a brief review of a new ketolide antibiotic. J. Drugs Dermatol 3, 409–413 (2004). [PubMed: 15303785]

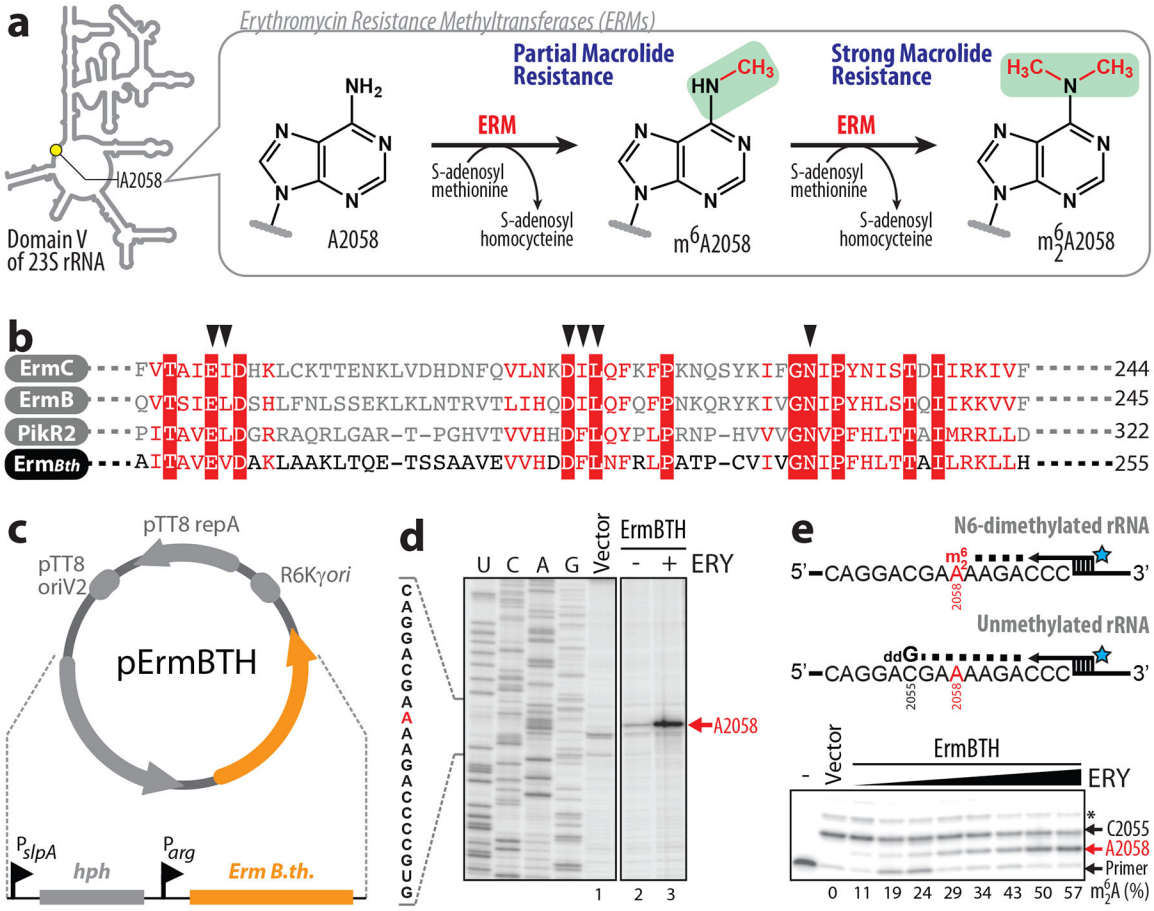

Figure 1 |. *Thermus thermophilus* HB27 strain expressing Erm-like methyltransferase.

(**a**) Mono- and dimethylation of the A2058 residue in the domain V of the 23S rRNA by the Erm-class methyltransferases results in high-level resistance to macrolides. (**b**) Multiple sequence alignment of several known Erm-methyltransferases from mesophilic bacteria (ErmC (*Staphylococcus aureus*), ErmB (*Streptococcus pneumonia*), and PikR2 (*S. venezuelae*)) with the Erm-like protein from moderately thermophilic *B. thermophilum* (ErmBth, optimal growth temperature 40–45°C). For complete sequence alignment, refer to Supplementary Fig. 2. A part of the amino acid sequences responsible for the binding of the donor of methyl groups (SAM) is shown. Conserved residues are highlighted in red. Black triangles point to the amino acid residues that coordinate SAM at the active site of the enzymes. (**c**) Schematic map of the plasmid vector used for the expression of ErmBth methyltransferase in *Thermus thermophilus* (*Tth*) HB27 cells. This vector designed to replicate in *Tth* carries the hygromycin B resistance marker *hph* under the control of P_{slpA} promoter (grey) and the ErmBth gene under the control of P_{arg} promoter (orange). (**d**) Primer extension analysis of the A2058-dimethylation in the 23S rRNA isolated from Erm(+) *Tth* cells. Cells transformed either with the empty pBGAA1 vector (lane 1) or with the pErmBTH plasmid were grown in the absence (lane 2) or in the presence of 0.5x MIC of ERY (lane 3). Reverse transcriptase stalls at N6-dimethylated A2058 and produces truncated cDNA (marked with the red arrow). Sequencing lanes are shown. (**e**) ErmBth-catalyzed A2058 dimethylation is stimulated by ERY in the growth medium. The concentration of

ERY was varied from 1/128 to 1/2 MIC, and cells were grown at 48°C. The isolated rRNA was analyzed by primer extension in the presence of dATP, dCTP, dTTP, and ddGTP. While the dideoxynucleotide ddGTP causes reverse transcription to stop at position C2055 on all templates, the N6-dimethylation arrest cDNA synthesis at position A2058 of the 23S rRNA. The reason for the appearance of the ‘readthrough’ cDNA product (indicated by an asterisk) is unclear but could result from either contamination of the reaction with dGTP, or nucleotide misincorporation at C2055 during reverse transcription at 50°C. The extent of dimethylation is calculated as a ratio of the intensity of the A2058-specific band to the sum of the intensities of the A2058-, C2055- and the readthrough bands (after background subtraction) and indicated below the gel. Experiments were repeated twice independently with similar results.

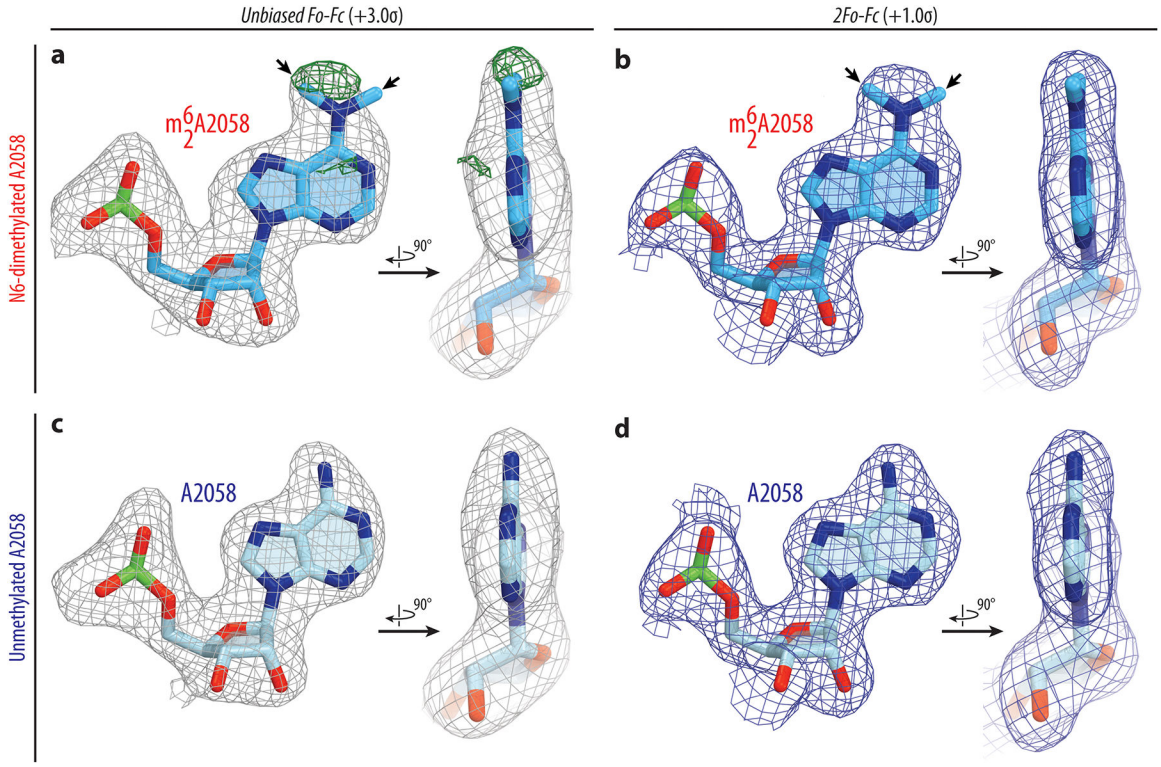

Figure 2 |. Electron density maps of N6-dimethylated (top) and unmethylated (bottom) A2058 residue of the 23S rRNA in *T. thermophilus* 70S ribosome.

(**a, c**) Unbiased F_o-F_c (grey and green mesh) and (**b, d**) 2F_o-F_c (blue mesh) electron difference Fourier maps of A2058 residue in the *T. thermophilus* 70S ribosome contoured at 3.0σ and 1.0σ, respectively, and viewed from two different perspectives. Grey mesh shows the F_o-F_c map after refinement with the entire modified nucleotide omitted. Green mesh, reflecting the presence of methyl groups, shows the F_o-F_c electron density map after refinement with the nucleotide A2058 built as a regular unmethylated adenine. The refined models of N6-dimethylated (a, b) or unmethylated (c, d) adenine nucleotide are displayed in the corresponding electron density maps. Carbon atoms are colored blue for the methylated A2058 and light blue for the unmethylated A2058; nitrogens are dark blue; oxygens are red, phosphorus atoms are green.

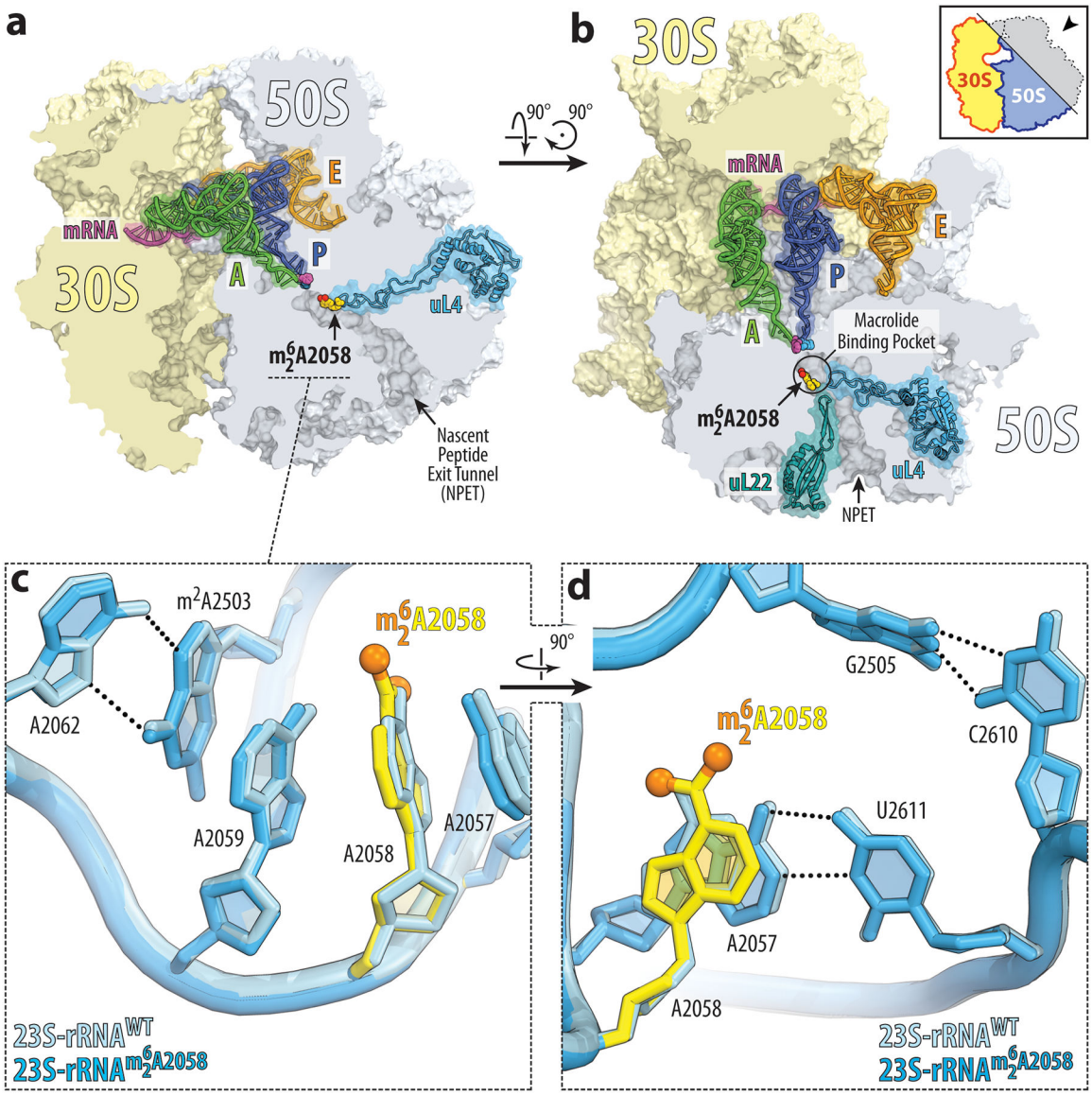

Figure 3 |. Structure of the Erm-modified 70S ribosome reveals the absence of any significant rearrangements in the macrolide binding pocket.

(**a, b**) Location of the Erm-modified nucleotide A2058 (yellow) carrying two methyl groups (orange) in the nascent peptide exit tunnel (NPET) of the *Tth* 70S ribosome relative to tRNAs and ribosomal proteins L4 (teal) and L22 (blue) viewed as cross-cut sections through the ribosome. The 30S subunit is shown in light yellow, the 50S subunit is in light blue, the mRNA is in magenta, and the A-, P-, and E-site tRNAs are colored green, dark blue, and orange, respectively. The phenylalanyl and formyl-methionyl moieties of the A- and P-site tRNAs are colored magenta and blue, respectively. (**c, d**) Close-up views of the 23S rRNA nucleotides lining the macrolide binding pocket in the NPET. Nucleotides of the Erm-modified and unmodified ribosomes are shown in blue and light blue, respectively. The N6-dimethylated A2058 residue is highlighted in yellow with methyl groups shown in orange. *E. coli* nucleotide numbering is used. H-bonds are shown with dashed lines.

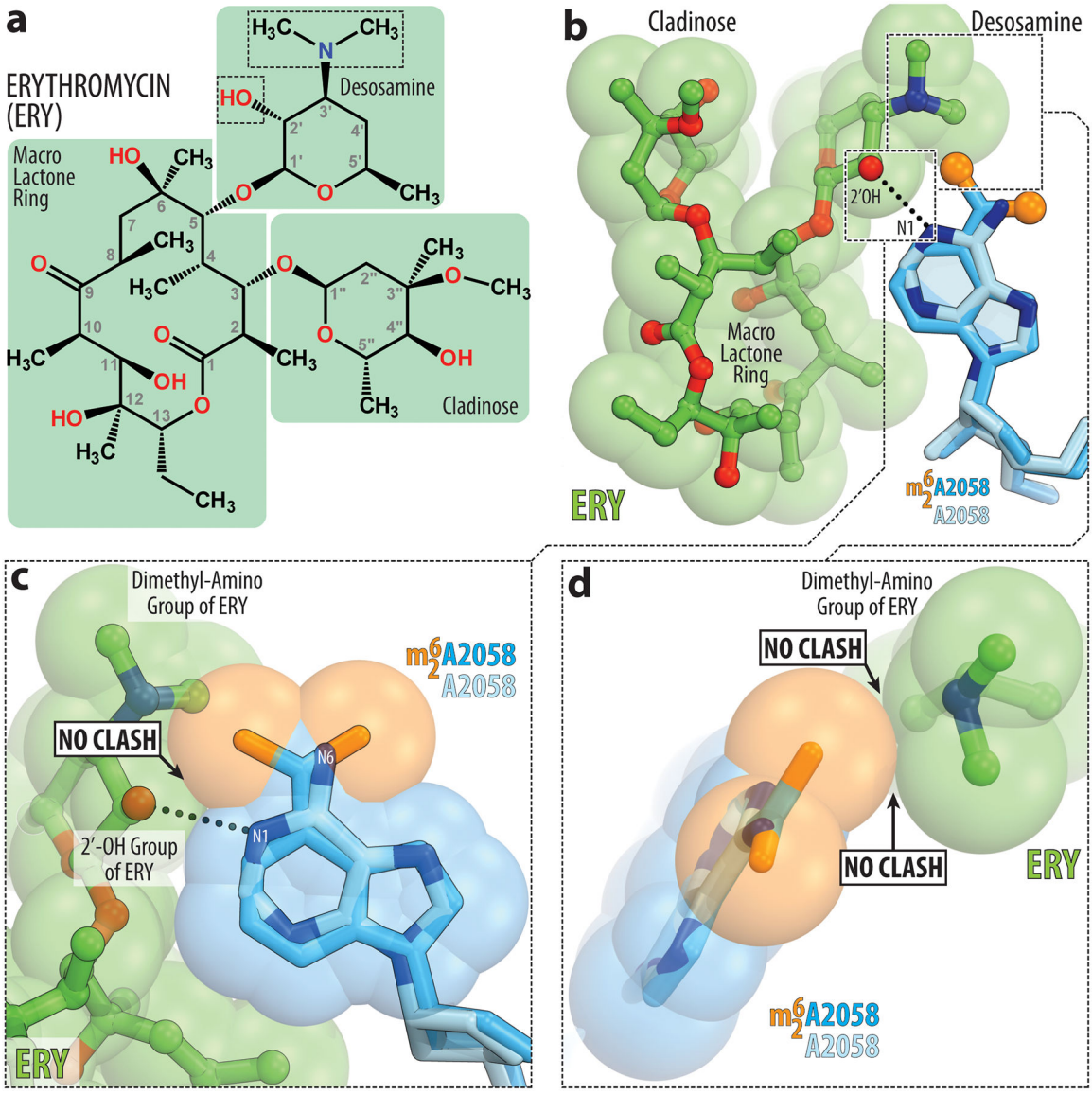

Figure 4 |. Superposition of the structures of A2058-methylated 70S ribosome and unmethylated 70S ribosome-ERY complex.

(**a**) Chemical structure of classical macrolide antibiotic erythromycin (ERY). The standard numbering of carbon atoms is shown in grey. (**b**) Superposition of the current structure of A2058-methylated 70S ribosome with the new high-resolution structure of ribosome-bound ERY. Methylated A2058 residue is shown in blue with the methyl groups highlighted in orange. Unmethylated A2058 residue is shown in light blue. All structures were aligned based on domain V of the 23S rRNA. (**c, d**) Close-up views of the desosamine 2′-OH group (c) and the desosamine dimethyl-amino moiety (d) relative to the methyl groups on $m^6{}_2$A2058 residue. Note that there are no sterical clashes between the methyl groups of $m^6{}_2$A2058 and the desosamine 2′-OH group (c) or the desosamine dimethyl-amino moiety (d) of ERY.

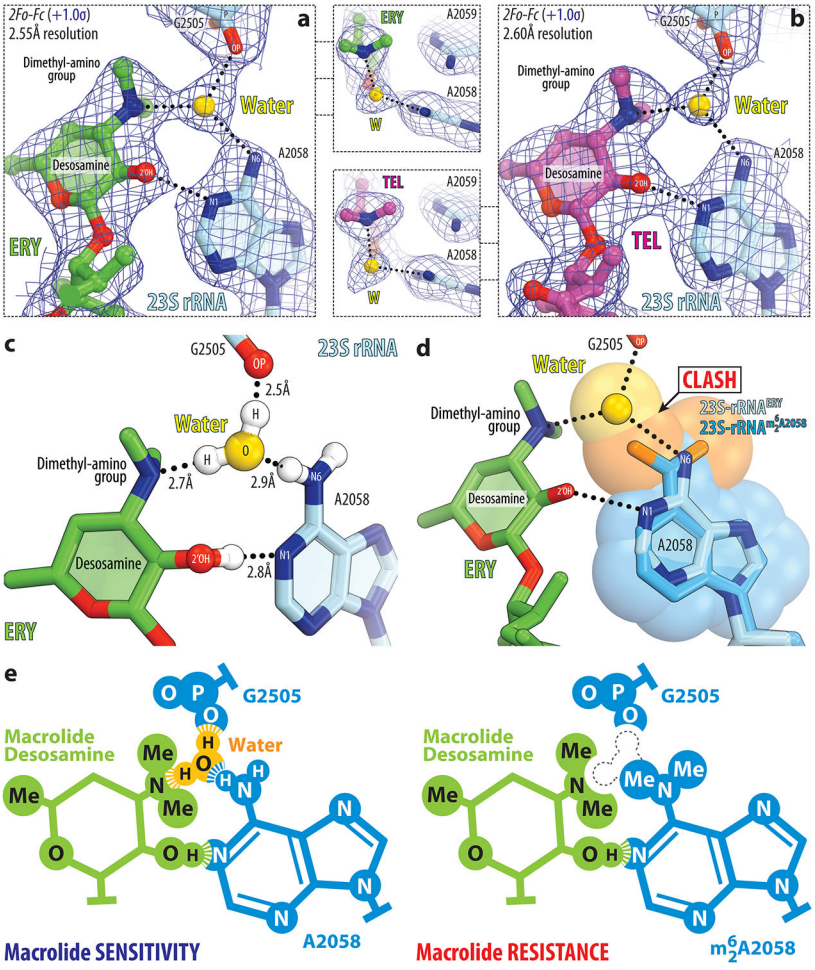

Figure 5 |. A water molecule mediates the interaction of macrolides with the ribosome.

(**a, b**) High-resolution $2F_o$-F_c electron density maps (blue mesh) of ribosome-bound ERY (green, A) and TEL (magenta, B) show that the dimethyl-amino group of a macrolide is rotated towards A2058 and forms an H-bond with a water molecule (yellow) that is tightly coordinated by the exocyclic N6-amino group of A2058 and the phosphate of G2505. The view in the middle insets is from the top along the H-bond, connecting the G2505 phosphate with the water. (**c**) Detailed arrangement of the H-bonds formed by the desosamine sugar of a macrolide (green) with 23S rRNA (blue) of the ribosome via a water molecule (yellow). Hydrogens are colored white; nitrogens blue; oxygens red (except for the water). H-bonds are shown with dashed lines. (**d**) Superpositioning of the new structures of ribosome-bound ERY with the new structure of the A2058-dimethylated 70S ribosome showing the clash between one of the m_2^6A2058 methyl groups and the water molecule. (**e**) Schematic diagram showing the molecular mechanism of resistance of A2058-dimethylated ribosomes to macrolide antibiotics. Note that due to the inability of the dimethyl-amino group of the $m^6{}_2$A2068 residue to serve as an H-bond donor, it cannot participate in the coordination of the water molecule on the ribosome. Moreover, the methyl groups physically displace the water molecule leaving the G2505 phosphate and the dimethyl-amino group of macrolide desosamine without an H-bond partner.